Local Effects of the Lithium Insertion into Cation-Deficient Tin−Indium Thiospinels Revealed by ^{119}Sn Mössbauer Spectroscopy

M. L. Elidrissi Moubtassim,[†] C. Bousquet, J. Olivier-Fourcade, and J. C. Jumas*

Laboratoire de Physicochimie de la Matière Condensée, UMR 5617 (CNRS), Université Montpellier II, Place E. Bataillon 34095, Montpellier Cedex 05, France

J. L. Tirado

Laboratorio de Química Inorgánica, Facultad de Ciencias, Universidad de Córdoba, San Alberto Magno s/n, 14004 Córdoba, Spain

Three thiospinel phases of the In_2S_3−SnS−SnS_2 system solid solution domain have been selected for electrochemical lithium insertion and local investigation by means of ^{119}Sn Mössbauer spectroscopy. Two distinct insertion mechanisms, characterized by two plateaus, are evident from the obtained discharge curves. Mössbauer spectroscopy and X-ray diffraction results are consistent with this. The first insertion mechanism is characterized by the reduction of Sn^{IV} and a cell expansion while the second one leads to an increased metallic-type Sn/Li interaction and a cell contraction, both accompanied by a migration of indium from tetrahedral to octahedral sites. The evolution of the hyperfine parameters is discussed to characterize the main differences between the three phases in terms of local and global guest−host interactions.

Introduction

Redox properties are based on the electronic transfer within the one-phase systems. Such systems are favorable to insertion mechanisms and are used as electrodes in rechargeable batteries. The insertion mechanisms are usually governed by different factors such as the rigidity of the host material, the presence of vacant sites able to receive the guest entities, and the aptitude of the network to absorb the associated electrons. The performance of an electrode material depends essentially on the amount of inserted entities (mass capacity), the efficient diffusion within the host matrix (ionic conduction path), and the good reversibility of the mechanism (cycling performance).

Three-dimensional materials were found to be of much interest as host lattices for insertion. Their many advantages have been underlined in many papers.[1] Typical examples are the spinel-structured phases which have been widely used for the development of lithium-based batteries.[1−6] The concept of using the $[B]_2X_4$ framework of the $A[B]_2X_4$ spinels as an insertion host was demonstrated several years ago. A common behavior has been observed in solids with this stoichiometry for which the host framework $[B]_2X_4$ remains unaltered after insertion while the A ions are displaced toward an extra set of sites.[7] However, cation deficient thiospinels with $A_y[B]_2X_4$ $(1 > y > 0)$ stoichiometry exhibit a different behavior; thus, a higher lithium mobility and an increased cycling performance have been reported.[4,8,9] Regarding their host capacity occurring without structural changes or repulsion, it is defined by the available sites, namely eight octahedral sites increased by the number of the tetrahedral vacancies.

The defect spinel In_2S_3 (with the extended formula: $(In_{5.33}\square_{2.66})[In_{16}]S_{32}$, parentheses and brackets represent tetrahedral and octahedral sites respectively, $\square$ the tetrahedral vacancy) and its solid solutions in the SnS−In_2S_3−SnS_2 pseudoternary system are typical examples of cation-deficient spinel compounds with cation vacancies in 8a sites of the $Fd\bar{3}m$ space group.[10] In addition, more interest is focused actually on tin-containing materials as electrode candidates.[11−13]

[†] On leave from Laboratoire des Sciences des Matériaux, Département de Physique, Faculté des Sciences SEMLALIA, Marrakesh, Morocco.
(1) James, A. C. W. P.; Goodenough, J. B. *Solid State Ionics* **1988**, *127*, 45.
(2) Eisenberg, M. *J. Electrochem. Soc.* **1980**, *127*, 2382.
(3) Chen, C. J.; Greenblatt, M.; Waszczak, J. V. *Mater. Res. Bull.* **1986**, *21*, 609.
(4) de la Mora, P.; Goodenough, J. B. *J. Solid State Chem.* **1987**, *70*, 121.
(5) Liu, W.; Farrington, G. C.; Chaput, C.; Dunn, B. *J. Electrochem. Soc.* **1996**, *143*, 879.
(6) Xia, Y.; Yoshio, M. *J. Electrochem. Soc.* **1996**, *143*, 825.

(7) Thackeray, M. M.; David, W. I. F.; Bruce, P. G.; Goodenough, J. B. *Mater. Res. Bull.* **1982**, *18*, 461.
(8) James, A. C. W. P.; Goodenough, J. B. *J. Solid State Chem.* **1987**, *70*, 121.
(9) Imanishi, N.; Inoue, K.; Takeda, Y.; Yamamoto, M. *J. Power Sources* **1993**, *43−44*, 619.
(10) Adenis, C.; Olivier-Fourcade, J.; Jumas, J. C.; Philippot E. *Rev. Chim. Minér.* **1987**, *25*, 10.
(11) Fuji Photo Film Co. European Patent EP0704921 A1, 1996.
(12) Idota, Y.; Kubota, T.; Matsufuji, A.; Maekawa, Y.; Miyasaka, T. *Science* **1997**, *276*, 1395.
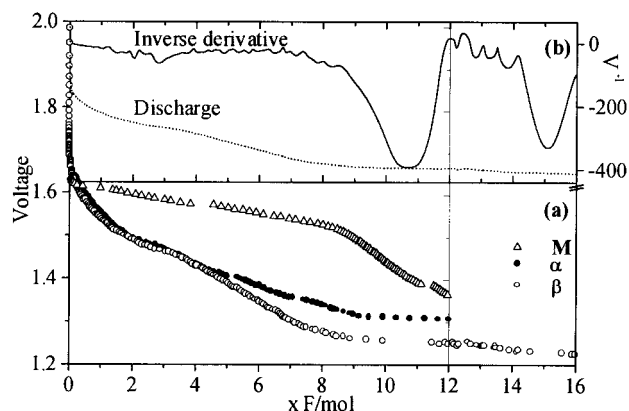
Recently, we have reported a lithium insertion study on one defect-spinel phase of this system.[14] The main objective was the study of its electrochemical behavior in comparison with that of the filled-tetrahedral site spinel $Cu_4In_{20}S_{32}$ to bring the influence of the deficiency on the insertion properties. The present work deals with the influence of the cation oxidation state in the pristine material on both the insertion mechanism and the guest−host interaction.

In this optic, we have chosen three compositions of the solid solution range, represented by the general formula $(In, \square)_8[In, Sn^{II}, Sn^{IV}]_{16}S_{32}$ with various Sn^{II}/Sn^{IV} ratios, to demonstrate how the lithium insertion is sensitive to the presence of tin under one or two oxidation states in the host network. Lithium insertion has been carried out electrochemically and the obtained samples characterized by X-ray diffraction and ^{119}Sn Mössbauer spectroscopy to bring both structural and local evolutions in addition to the electrochemical data.

Experimental Section

The samples under study have been synthesized by solid-state reactions between the binary sulfides mixed in stoichiometric proportions. The mixtures, placed under high vacuum, were heated at 700 °C for 5 days. The first sample prepared from In_2S_3 and SnS_2 in the molar ratio 2:1 has been cooled gradually to the room temperature to stabilize the low-temperature ordered form (red) based on $\beta\text{-}In_2S_3$[15,16] with one tin-valence and the extended formula $(In_4\square_4)[In_{12}Sn_4^{IV}]S_{32}$. The two others have been prepared from the sulfides In_2S_3, SnS, SnS_2 in the molar ratios 2:0.05:0.95 and 2:0.35:0.65. They have been quenched in water to obtain the high-temperature disordered forms (black) based on the cubic $\alpha\text{-}In_2S_3$ with two tin valences and the extended formulas $(In_{4.16}\square_{3.83})[In_{12.10}Sn_{0.19}^{II}Sn_{3.71}^{IV}]S_{32}$ and $(In_{4.93}\square_{3.06})[In_{11.91}Sn_{1.44}^{II}Sn_{2.65}^{IV}]S_{32}$, respectively. To simplify the samples' description we will use, in the following sections, the formula notations: $\beta\text{-}In_{16}Sn_4S_{32}$ for the one tin-valence phase, $\alpha\text{-}In_{16.26}Sn_{3.90}S_{32}$ for the two tin-valences phase with the composition ratio 2:0.05:0.95, and $M\text{-}In_{16.84}Sn_{4.09}S_{32}$ for the composition ratio 2:0.35:0.65. The resulting crystalline powders were found, by X-ray diffraction, to be pure with lattice parameters of 10.700(1) Å for the α- and β-phases (note that their chemical compositions are close to each other) and 10.753(4) Å for the M-phase. ^{119}Sn Mössbauer spectra consisted of one split-line characteristic of Sn^{IV} for $\beta\text{-}In_{16}Sn_4S_{32}$, two subspectra characteristic of Sn^{IV} (96% contribution) and Sn^{II} (4% contribution) for $\alpha\text{-}In_{16.26}Sn_{3.90}S_{32}$, and two subspectra characteristic of Sn^{IV} (68% contribution) and Sn^{II} (32% contribution) for $M\text{-}In_{16.84}Sn_{4.09}S_{32}$. The use of the Lamb−Mössbauer factors relative to Sn^{II} and Sn^{IV} (0.61 and 0.71 respectively) determined previously for such materials[17] leads to the Sn^{II}/Sn^{IV} ratios which have been found of 0.05 and 0.55 for α-phase and M-phase, respectively.

The electrochemical experiments were carried out in $Li/LiClO_4(PC)$ (1 M)/spinel cells prepared in a drybox (M. Braun) by placing a lithium metal disk, glass fiber separators soaked with the electrolyte solution, and a pellet of the concerned spinel into a Teflon container with two stainless steel terminals. The cell is connected to a multichannel galvanostatic/potentiostatic system (MacPile) controlled by a microprocessor. The cathode pellets (7 mm diameter) were prepared by

(13) Courtney, I. A.; Dahn, J. R. *J. Electrochem. Soc.* **1997**, *144−6*, 2045.
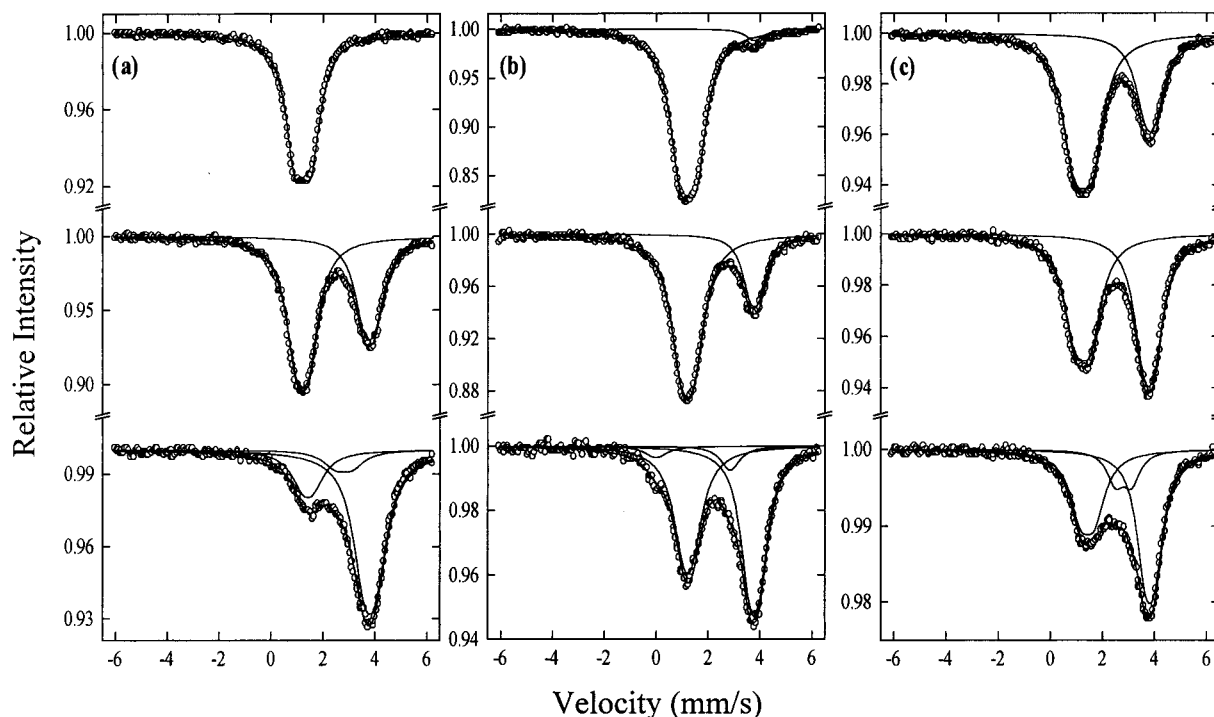
(14) Morales, J.; Tirado, J. L.; Elidrissi Moubtasim, M. L.; Olivier-Fourcade, J.; Jumas, J. C. *J. Alloys Compd.* **1995**, *217*, 176.

(15) Elidrissi Moubtassim, M. L.; Olivier-Fourcade, J.; Jumas, J. C.; Maurin, M. *J. Solid State Chem.* **1990**, *87*, 274.

(16) Diehl, R.; Nitsche, R., *J. Cryst. Growth* **1975**, *28*, 306.

(17) Elidrissi Moubtassim, M. L.; Olivier-Fourcade, J.; Jumas, J. C. *Eur. J. Solid State Inorg. Chem.* **1991**, *28*, 1307.

Figure 1. Continuous intensiostatic discharge curves carried out at 38 μA for the three phases (a). The inverse derivative (dx/dV) of $\beta\text{-}Li_xIn_{16}Sn_4S_{32}$ discharge curve up to 16 F/mol (b).
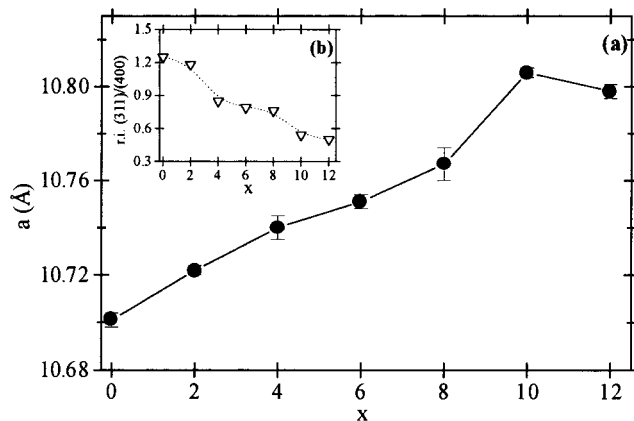
Figure 2. Cell parameter (a) and the (311)/(400) relative intensity ratio (b) variation vs the lithium content for $\alpha\text{-}Li_x In_{16.26}Sn_{3.90}S_{32}$.

pressing 25−30 mg of the compound without additive matter. An initial relaxation of the cells was allowed until the condition $\Delta V/\Delta t < 1$ mA h^{-1} was attained. The average lithium content of the cathode material was calculated from the amount of electron charge transferred to the active material, on the assumption that no current flow was due to side reactions. Steps of 2 Li per 32 S formula have been chosen to allow a progressive study of the evolution of the host material. After each lithium insertion step, the pellet was extracted from the cell inside the drybox and protected with a plastic film to avoid any contact with air during the subsequent characterization experiments.

X-ray powder diffraction was carried out by means of a PHILIPS diffractometer working with Cu $K\alpha$ radiation. ^{119}Sn Mössbauer spectra were recorded in the constant-acceleration mode on an ELSCINT-AME40 spectrometer. The γ-ray source ($Ba^{119m}SnO_3$) is kept at room temperature while the samples under study were cooled to 77 K in a liquid nitrogen circulation cryostat. The velocity scale was calibrated with the magnetic sextet spectrum of a high-purity iron foil absorber and a $^{57}Co(Rh)$ source. Recorded spectra were fitted to Lorentzian profiles by a least-squares method[18] and the fit quality controlled by the usual χ^2 and misfit tests. The origin of the isomer shifts is determined from the center of the $BaSnO_3$ absorber spectrum recorded under the same experimental conditions as the studied samples.

Results and Discussion

Electrochemical Study. Typical intensiostatic discharge curves at 38 μA are shown in Figure 1. They

(18) Kundig, W. *Nucl. Instr. Methods* **1969**, *75*, 336.

Figure 3. Typical recorded and fitted ^{119}Sn Mössbauer spectra: β-Li$_x$In$_{16}$Sn$_4$S$_{32}$ (a), α-Li$_x$In$_{16.26}$Sn$_{3.90}$S$_{32}$ (b), M-Li$_x$In$_{16.84}$Sn$_{4.09}$S$_{32}$ (c). $x = 0$, 4, and 12 from top to bottom.

Table 1. ^{119}Sn Mössbauer Parameters Recorded at 77 K for β-Li$_x$In$_{16}$Sn$_4$S$_{32}$ ($x = 0$, 4, 16)[a]

	Sn^{IV}				Sn^{II} (1)				Sn^{II} (2)			
x	δ (mm/s)	Δ (mm/s)	Γ (mm/s)	C (%)	δ (mm/s)	Δ (mm/s)	Γ (mm/s)	C (%)	δ (mm/s)	Δ (mm/s)	Γ (mm/s)	C (%)
0	1.126(3)	0.61(1)	0.88(2)	100								
4	1.111(5)	0.49(1)	0.95(2)	61	3.69(1)	0.42(2)	0.49(3)	39				
12	1.18(2)	0.44(4)	1.01(6)	20	3.719(9)	0.48(1)	1.01(2)	70	2.83(7)	0.58(1)	1.01(2)	10

[a] Isomer shifts are relative to BaSnO$_3$. Standard deviations are in parentheses.

are in good agreement with the results obtained by galvanostatic intermittent titration technique (GITT) and step potential electrochemical spectroscopy (SPES) of lithium cells described previously.[14] For the three phases, the continuous discharge curves consisted of an initial abrupt decrease in voltage followed by three consecutive plateaus for the one tin-valence phase (β), more clearly defined by the corresponding peaks in the plot of the derivative of the voltage (dV/dx) which is proportional to the cell incremental capacity. The first plateau occurs at 1.6 V for the M-phase and 1.4–1.5 V for the α and β phases. This behavior is consistent with the existence of two intercalation mechanisms, since the third plateau at about 1.2 V could correspond to an electrolyte reduction that occurs at this voltage for other sulfides but which also depends on the nature of the cathode material.[19] So, we limit the following analysis to the two first plateaus region, namely till 12 F/mol. The first one, associated to a high lithium diffusion,[14] is ascribed to a predominating insertion into the octahedral coordinated 16c sites of the spinel lattice which are particularly favorable to a good chemical diffusion of the guest entities. This set of sites shares faces with the tetrahedral coordinated 8a and 48f sites,[1,20] and then

it provides continuously interconnected spaces through which the lithium can diffuse more easily and allows a high further insertion capacity.

X-ray Diffraction. Powder X-ray diffraction diagrams provide additional information. The unit cell parameter increases for the three phases in the lithium content range $10 \geq x \geq 0$ (Figure 2). This behavior is usually observed in rigid host lattices[1-4] and corresponds to the first insertion process underlined in the electrochemical study section. For $x > 10$, a contraction of the cell, more marked for the mixed-valence phase, is observed. In this domain corresponding to a second insertion process, as indicated above, another set of sites is occupied. In addition, very significant changes in the reflection pattern intensities are evident. This has been reported in previous works[14] and also detected for other intercalation compounds.[1,4] The main representative illustration is the comparison of the (400) and (311) reflection intensities. Thus, the (400) reflection intensity increases while the (311) decreases with the lithium content. Example of the plot of the intensity ratio (r.i.-(311)/r.i.(400)) vs the lithium content illustrates this in Figure 2. Such changes are related to the diffusion of strongly scattering cations from tetrahedral to octahedral sites. In this case, only the indium is able to diffuse since all tin atoms are located in octahedral sites.[21]
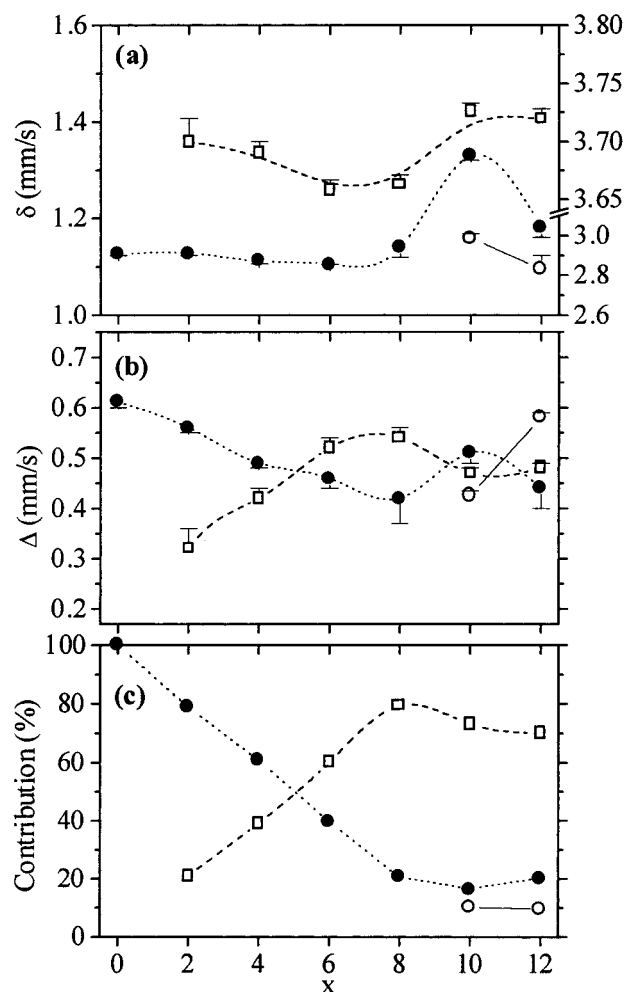
^{119}Sn Mössbauer Spectroscopy. To simplify the presentation of the Mössbauer results, let us give first

(19) McMillan, R. C.; Juskow, M. W. *Proc. Electrochem. Soc.* **1990**, *90–5*, 149.

(20) James, A. C. W. P.; Goodenough, J. B. *J. Solid State Chem.* **1988**, *77*, 356.

a brief survey of the most important hyperfine parameters and some common points to the three phases. Then, we will present the discussion for each phase. The isomer shift (δ) which is related to the electron density at the probe nucleus (tin) provides valuable information on the short-range changes as the oxidation state, the bonding nature, and the coordination. The quadrupole splitting (Δ) depends essentially on the local electric field gradient, so it is directly influenced by any changes in the site symmetry, the coordination, or the bonding state. For the three phases (α, β, and M), two fitting modes have been used to analyze the recorded spectra. In the range 8 (or 10) $\geq x > 0$, two split-lines, arising from the coexistence of Sn^{IV} and Sn^{II}, within octahedral environments allow the fit to be achieved. Beyond 8 (or 10) lithium-content a further subspectrum appears; thus, all the spectra have been fitted with three lines. The existence of these two domains is well consistent with the electrochemical and X-ray results in term of the existence of two insertion mechanisms corresponding to the two lithium-content domains cited above.

One Tin-Valence Thiospinel β-In$_{16}$Sn$_4$S$_{32}$. Figure 3a shows typical recorded and calculated spectra corresponding to the pristine material and inserted ones belonging to the two insertion domains. The relevant parameters are assembled in Table 1. Note that the spectrum of the noninserted phase consists of one split-line with hyperfine parameters characteristic of Sn^{IV} in a little-distorted octahedral site ($\delta = 1.126(3)$ mm/s, $\Delta = 0.61(1)$ mm/s) in agreement with previous results.[22–25] After insertion, an evident reduction of Sn^{IV} to Sn^{II} takes place since the spectra show a second subspectrum (10 $\geq x > 0$) or two additional subspectra ($x > 10$) with hyperfine parameters characteristic of tin at the oxidation state II. The relative contribution of the Sn^{IV} subspectrum decreases linearly when x increases (Figure 4c) up to eight Li per formula (first insertion domain) and remains invariant beyond. This is in agreement with the reduction process observed previously in similar phases inserted chemically.[21] Sn^{IV} isomer shift (δ) remains practically invariant up to $x = 8$. However, the quadrupole splitting (Δ) decreases in this domain. We conclude that the insertion mechanism takes place without strong short-range modifications on Sn^{IV} centers of which the environment becomes as more regular as the lithium content increases. In the second domain ($x > 8$) the isomer shift (δ) and the quadrupole splitting (Δ) variation are similar and reflect a little gain of electron density at this nucleus accompanied by a weak symmetry loss (Figure 4a,b). Concerning Sn^{II} parameters, we note the existence of the two mentioned domains. For 10 $\geq x > 0$, one Sn^{II}-type is present, its isomer shift varies slightly with the lithium content and its site symmetry goes down since Δ increases. For $x = 10$ and more, a second Sn^{II}-type appears. The first one (we will note $Sn^{II}(1)$) does not present strong local

(21) Elidrissi Moubtassim, M. L.; Olivier Fourcade, J.; Senegas, J.; Jumas, J. C. *Mater. Res. Bull.* **1993**, *28*, 1083.
(22) Padiou, J.; Jumas, J. C.; Ribes, M. *Rev. Chim. Minér.* **1981**, *18*, 33.
(23) Adenis, C.; Olivier-Fourcade, J.; Jumas, J. C.; Philippot, E. *Rev. Chim. Minér.* **1986**, *23*, 75.
(24) Adenis, C.; Olivier-Fourcade, J.; Jumas, J. C.; Philippot, E. *Rev. Chim. Minér.* **1987**, *24*, 10.
(25) Adenis, C.; Olivier-Fourcade, J.; Jumas, J. C.; Philippot, E. *Eur. J. Solid State Inorg. Chem.* **1988**, *25*, 413.

Figure 4. Isomer shift (a), quadrupole splitting (b), and subspectra contribution (c) evolutions with the lithium content for β-Li$_x$In$_{16}$Sn$_4$S$_{32}$. (●) Sn^{IV}, (□) Sn^{II}_1, (○) Sn^{II}_2.

modifications. Thus, its isomer shift stands out against the obtained value at $x = 8$, but remains almost invariant. The quadrupole-splitting variation reflects a very weak modification of its site symmetry. The second Sn^{II}-type (we will note $Sn^{II}(2)$) gives rise to a subspectrum located, in terms of isomer shift, in an intermetallic domain (Figure 3a). Associated hyperfine parameters (δ and Δ) are characteristic of covalent Sn^{II} (Table 1). The decrease of δ and increase of Δ when the lithium content increases indicate that the Sn^{II} electron lone pair becomes more and more active, leading to the loss of the Sn^{II} site symmetry and the enhancement of its bonding covalence. This behavior is typical of the enhanced like-metallic interaction between tin and lithium.

Two Tin-Valence Thiospinel α-In$_{16.26}$Sn$_{3.90}$S$_{32}$. For this phase, the Mössbauer spectrum (Figure 3b) of the starting material consists of two split-lines relative to Sn^{IV} (δ and Δ similar to those of β-In$_{16}$Sn$_4$S$_{32}$) and Sn^{II} both located in the little-distorted octahedral site, with a contribution of 4% for the latter (Table 2). Within the explored insertion domain, no significant changes have been noted for the Sn^{IV} isomer shift (Figure 5a), which is still around an average value of 1.12 mm/s. So, the Sn^{IV} electron density and bonding state are not as altered as in the β-phase. However, the decrease of Δ reveals subsequent changes of its

Table 2. ^{119}Sn Mössbauer Parameters Recorded at 77 K for α-Li$_x$In$_{16.26}$Sn$_{3.90}$S$_{32}$ (x = 0, 4, 16)^a

	Sn^{IV}				Sn^{II} (1)				Sn^{II} (2)			
x	δ (mm/s)	Δ (mm/s)	Γ (mm/s)	C (%)	δ (mm/s)	Δ (mm/s)	Γ (mm/s)	C (%)	δ (mm/s)	Δ (mm/s)	Γ (mm/s)	C (%)
0	1.124(3)	0.61(1)	0.96(2)	96	3.69(5)	0.26(9)	0.70(9)	4				
4	1.103(6)	0.48(1)	1.01(2)	75	3.69(1)	0.36(2)	0.76(3)	25				
12	1.12(2)	0.34(4)	1.02(9)	41	3.68(1)	0.40(2)	0.87(2)	50	2.75(4)		0.87(3)	6

^{a} Isomer shifts are relative to BaSnO$_3$. Standard deviations are in parentheses.

Table 3. ^{119}Sn Mössbauer Parameters Recorded at 77 K for M-Li$_x$In$_{16.84}$Sn$_{4.09}$S$_{32}$ (x = 0, 4, 16)^a

	Sn^{IV}				Sn^{II} (1)				Sn^{II} (2)			
x	δ (mm/s)	Δ (mm/s)	Γ (mm/s)	C (%)	δ (mm/s)	Δ (mm/s)	Γ (mm/s)	C (%)	δ (mm/s)	Δ (mm/s)	Γ (mm/s)	C (%)
0	1.152(4)	0.67(1)	1.08(2)	68	3.73(2)	0.37(2)	0.98(3)	32				
4	1.23(2)	0.49(4)	1.14(5)	40	3.67(1)	0.46(2)	1.01(3)	60				
12	1.38(2)	0.44(4)	1.00(4)	24	3.73(1)	0.44(1)	0.88(2)	54	2.65(5)	0.66(4)	1.00(8)	22

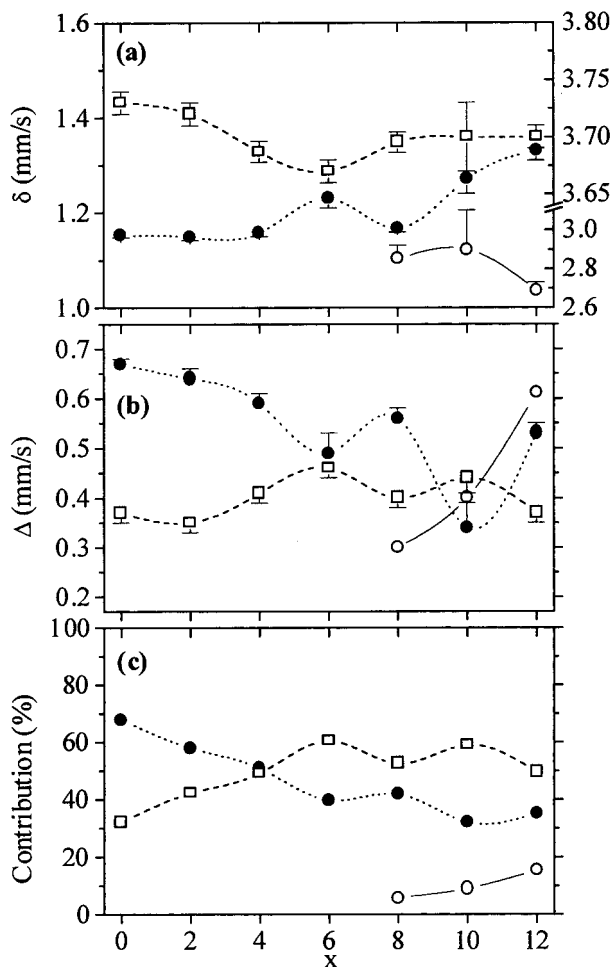^{a} Isomer shifts are relative to BaSnO$_3$. Standard deviations are in parentheses.
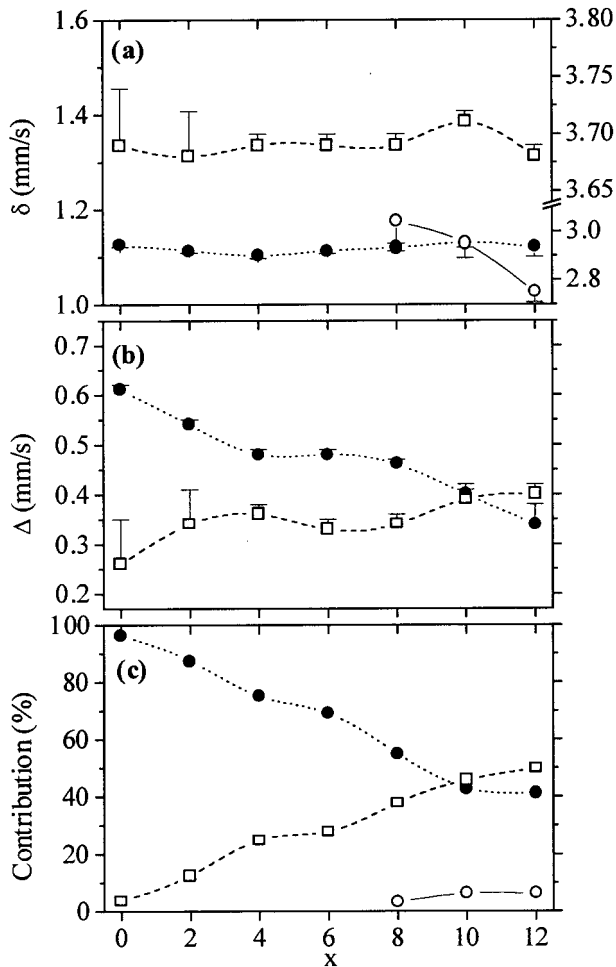
Figure 5. Isomer shift (a), quadrupole splitting (b), and subspectra contribution (c) evolutions with the lithium content for α-Li$_x$In$_{16.26}$Sn$_{3.90}$S$_{32}$. ($\bullet$) Sn^{IV}, ($\square$) Sn$_1^{II}$, ($\bigcirc$) Sn$_2^{II}$.

environment symmetry (Figure 5b). The Sn^{IV} contribution decreases quasi-linearly when x increases without marked separation between the two insertion domains. In addition, the slope is weaker than that observed for the β-phase. Therefore, the Sn^{IV} reduction going with the lithium insertion is less strong in this case. Note that the decrease of the Sn^{IV} contribution (due to its reduction) stops at 41% (Figure 5c) while it goes until 20% for the one tin-valence phase. Concerning Sn^{II}(1) the isomer shift is almost constant (around 3.69 mm/s)

over the entire prospected lithium content domain. As concluded for Sn^{IV}, there is no significant modification at the Sn^{II}(1) sites except a weak increase noted for Δ. The Sn^{II}(2) Mössbauer-effect peak appears here from x = 8. Its isomer shift decreases as in the β-phase in relation with the increase of the covalence. The thinness of the corresponding subspectra does not allow the use of split-lines. Thus, the Sn^{II}(2) sites are at least much more regular than in the β-phase. The insertion process observed by tin as a probe is quite different from the α- to β-phase in terms of local electronic changes. The only common points are the Sn^{IV} to Sn^{II} qualitative reduction and the existence of the two insertion domains indicated in the β-phase by the variation of the hyperfine parameters, while only the appearance of Sn^{II}(2) Mössbauer subspectra reveals it for the α-phase.

Two Tin-Valence Thiospinel M-In$_{16.84}$Sn$_{4.09}$S$_{32}$. Representative experimental and calculated spectra of this phase, before and after lithium insertion, are shown in Figure 3c. The corresponding parameters are assembled in Table 3. As indicated above, this phase is a mixed valence one, so, the noninserted compound spectrum is composed by two split-lines characteristic of Sn^{IV} and Sn^{II} both in octahedral sites, with a subspectra-contribution ratio C(Sn^{II})/C(Sn^{IV}) = 0.47. From the Figure 6a, one can discern two Sn^{IV} isomer shift-variation domains. Untill x = 8, δ is quasi-invariant whereas it increases beyond. This indicates that the enhancement of the Sn^{IV} electron density during the second insertion mechanism is stronger than the one occurring in the two other phases. The Sn^{IV} quadrupole-splitting evolution presents a regular decrease up to x = 6 (Figure 6b) and becomes irregular beyond. About the Sn^{IV} subspectra contribution, the decrease is linear until x = 6 (Figure 6c). The value reached at x = 12 is 35%. The Sn^{II}(1) isomer shift decreases also up to x = 6 and remains practically constant between 8 and 12. Regarding the quadrupole splitting, it increases also up to x = 6 and varies weakly beyond. For this phase, all the hyperfine parameters variation changes converge on the occurrence of the first insertion domain limit at x = 6. This earlier behavior is due to the presence of the reduced form of tin in the noninserted material, at a large amount, which slows the tin reduction and favors the increase of the network bond covalence. About Sn^{II}-(2), δ and Δ vary with x as in the β-phase, i.e., δ

Figure 6. Isomer shift (a), quadrupole splitting (b), and subspectra contribution (c) evolutions with the lithium content for $M-Li_xIn_{16.84}Sn_{4.09}S_{32}$. (●) Sn^{IV}, (□) Sn_1^{II}, (○) Sn_2^{II}.

decreases and Δ increases in agreement with the Sn^{II} electron lone pair activity, leading to a distortion of the site and an enhanced tin—lithium interaction.

Conclusion

The interpretation of a large lithium-amount reaction with tin-containing materials is of topical interest. In our case, it is clear, from the Mössbauer results, that the tin reduction is not the unique electron exchange mechanism, since the Sn^{II} contribution is not equivalent to the guest (Li^+/electrons) pairs and no complete reduction has been observed. In addition, we have performed both chemical and electrochemical lithium insertions into the solid solution-based phase In_2S_3 (a free-tin phase) with success. The main characterization results allow us to conclude a wide insertion capacity (determined by atomic absorption analysis), the lithium being at its ionic state as demonstrated by ^7Li NMR experiments. An interpretation of this partial tin reduction has been developed in a recent article[26] dedicated to the insertion mechanisms in these materials. A theoretical model based on a full tight-binding and tight-binding molecular levels methods has been proposed. The lithium ions have been considered as point defects inducing deep and shallow donor states in the gap according to the insertion site. It has been demonstrated that the deep donor state is unstable under local atomic distortions and exhibits negative U behavior. This situation leads to a collection of either doubly occupied or empty donor states which explains the complete reduction of a part of tin atoms while the others remain under their initial oxidation state.

In summary, the combination of different experimental and theoretical tools have allowed us to understand how these phases are able to accept the lithium and its associated guest electrons. Electrochemical, structural, and short-range properties have been examined. Results show that these host materials are of high insertion capacity without structural damage. It has been demonstrated that two intercalation phenomena are involved over the explored lithium-content range. Usual behaviors of rigid three-dimensional lattices, as the cell expansion/contraction and the cation migration from tetrahedral to octahedral sites have been detected. ^{119}Sn Mössbauer spectroscopy has played a key role in the local changes understanding. Thus, two competitive phenomena involving the guest electrons have been clearly defined: the Sn^{IV} to Sn^{II} partial reduction, and the increase of the covalence, related to an increasing metallic-type interaction between Sn and Li. The role of the tin oxidation state has been determined. This one, in addition to previous results, may allow a judicious selection of the phases with optimal properties as candidates for electrode materials.

(26) Lefebvre, I.; Lannoo, M.; Elidrissi Moubtassim, M. L.; Olivier-Fourcade, J.; Jumas, J. C. *Chem. Mater.*, accepted.